Hot Ductility Characterization of Low- and Medium-Carbon Steels

Hot ductility testing is a well-established method to investigate effects of alloying and casting conditions on slab surface sensitivity to cracking. In this work, the hot ductility of four different steel chemistries ranging in carbon content from 0.06 to 0.40 wt. % and with varying amounts of precipitate forming elements (e.g., Ti, Nb, V) are studied using a Gleeble 3800. Specimens prepared from continuously cast slabs were homogenized at 1,350°C for 5 minutes before cooling at 1°C/second to testing temperatures between 1,300°C and 600°C and then strained isothermally to failure with a rate of 1 x 10^{-3} second^{-1}. The reduced area of these tests was used to evaluate their hot ductility performance. Fractography on the tested specimens and metallography on quenched specimens after homogenization were performed. Alongside these experimental results, the Thermo-Calc predicted phase and precipitate stability are presented. Using these results, factors affecting hot ductility performance in these grades are discussed.

Authors

Michael J. Gaudet (left), Manager of Metallurgy, R&D, Interpro Pipe and Steel, Regina, Sask., Canada
michael.gaudet@interprosteel.com

Lorne Good, Senior Metallurgical Technologist, Interpro Pipe and Steel, Regina, Sask., Canada

Bikram Konar (right), Senior Research Engineer, Interpro Pipe and Steel, Regina, Sask., Canada

Introduction

The loss of ductility (high-temperature embrittlement) of steel has been reported from liquidus to above ~650°C. This hot ductility performance is associated with quality concerns in continuously cast (CC) steel products, such as hot tearing, transverse cracks, corner cracks and longitudinal cracks. Hot ductility testing typically uses the reduced area percentage (RA%) as measured by the decrease of original to final area of a round bar pulled in tension at high temperatures until fracture. These hot ductility tests have been useful in revealing the hot cracking propensity of a steel products due to various factors, including: alloying elements, physical caster and product parameters (caster design, cast product shape, casting speed, mold flux, mold fluid flow, etc.), and thermal conditions (primary cooling, secondary cooling, roll contact, etc.).

During the continuous casting process, strain rates[1] and cooling rates[2] impact the high-temperature embrittlement of steels. The high-temperature embrittlement in steels often occurs in two temperature regimes[3,4] including one near the solidus temperature and the other near Ae_3 (equilibrium austenite to α-ferrite transition). In the latter case, the loss of ductility may overlap with temperatures observed in the bending-unbending section in a curved CC operation. Known factors on hot ductility performance at these temperatures are shown schematically in Fig. 1 and are as follows:

a. Dynamic recrystallization (DRX) zone: above DRX temperature (TDRX)[5] triggers considerable amount of austenite phase grain refinement which can be hindered by precipitate formation along the grain boundaries as the temperature decreases.

b. Grain boundary sliding: prevalent at higher temperatures in the range of ~1,200°C to Ar_3 (nonequilibrium austenite decomposition temperature). At these temperatures, austenite with limited dynamic recovery and grain deformation incompatibility can result in intergranular failures. This mechanism is usually associated with creep and

is strain rate dependent (10^{-4} to 10^{-3} second^{-1}).[6] Generally, on increasing the strain rate, the ductility improves as the time available for grain boundary sliding is reduced.

c. Austenite-to-ferrite transition and related phenomenon:

   i. Precipitate formation: equilibrium- and deformation-induced precipitates (AlN, Nb(C,N)[7–10]) form along the austenite grain boundaries which generate near-grain boundary precipitate free zones. Strain concentration in these softer zones leads to microvoid formation/coalescence, leading to intergranular ductile fracture. This can occur in the austenite but may be made more pronounced at local sites of ferrite transformation.

   ii. Grain boundary ferrite formation: a ductility drop can be caused by soft ferrite film formation (deformation induced ferrite, DIF) at the austenite grains boundaries between Ae_3 and Ar_3 (influenced by alloying elements, cooling rate, strain rate–related precipitation of AlN and inclusions of MnS).[2,5,6,11,12]

d. Ferrite formation: ductility improves with the increasing presence of the more-ductile ferrite as the austenite decomposition progresses.

The elemental makeup of the steel is a significant factor in the hot ductility, though not always straightforward owing to how the microstructure may evolve in the course of casting. Thus, in terms of elements, the hot ductility of steel primarily depends on:

a. Carbon content as it strongly influences the primary steel phases (δ-ferrite, austenite and α-ferrite) formation and transition temperatures. Historically, empirical carbon equivalence (CE) formulae[13–15] have been used to capture the effects alloying elements on primary phase formation and transitions. The transition temperatures (e.g., δ-ferrite to austenite) and phase stability ranges (e.g., single-phase austenite region is observed at higher temperatures for near-peritectic steel grades) affects the hot ductility loss through previously discussed factors such as austenite grain coarsening that are associated with intergranular fractures.[16] The austenite formation is affected by C but also the austenite decomposition is largely controlled by C diffusion at relevant cooling rates.

b. Other alloying elements:[4,17,18]

   i. Microalloying elements like Ti, Nb, V and Al form carbides, nitrides and carbonitride precipitates that impact the thermokinetics of primary phase transitions. Both the presence of the precipitates and their influence on the phase transformation may be detrimental to hot ductility.

   ii. Nonmetallic impurities like S that forms MnS precipitates with different shapes (spheroids, cylindrical rods, and idiomorphic crystals/angular[19]) that are stable above steel solidus and increases susceptibility to cracking. Also, sulfur and phosphorus will strongly segregate and enrich interdendritic regions and grain boundaries.

   iii. Residual elements like Cu and Sn are prevalent in scrap-based steel products and cause hot shortness and reduce the hot ductility of steels.[17,20,21]

Figure 1

Schematic of a hot ductility curve of steel showing effects of recrystallization and the trough near Ae_3 potentially related to deformation induced ferrite (DIF).[2]

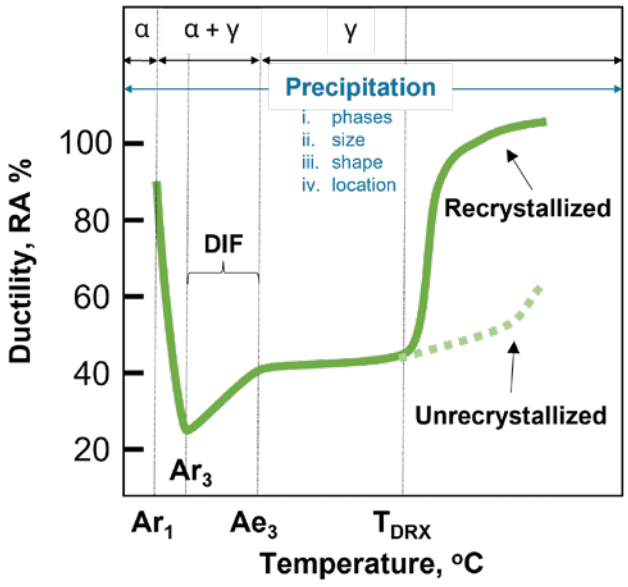

Understanding susceptibility to cracking during the secondary cooling in relation to alloying practices allows for the optimization of casting parameters. The present work examines the hot ductility performance near Ae_3 region for several steel grades with different carbon equivalent contents and alloying elements through the use of a hot tensile testing method to determine RA%. Metallography and fractography provide supporting information to the RA% data generated. Discussion of the formation and interaction of primary phases and precipitate phases and grain structures is aided through thermodynamic modeling and, in context of the literature, provides insight into the observed hot ductility results.

Experimental Procedure

Five steel grades that were industrially produced from a scrap-based electric arc furnace and continuously cast into thick slabs were investigated. In sampling the slabs from available transverse sections, samples were not taken from the narrow face edges nor from the centerline region to avoid effects related to segregation, as shown in Fig. 2a. Round bar samples of 116.5 mm length and 10 mm diameter were machined from blanks as cut from the as-cast slab aligned axially to the transverse direction as shown in Fig. 2b.

Hot ductility testing was performed on a Gleeble 3800 thermomechanical simulator using the program as shown schematically in Fig. 3. The testing program utilized a homogenization temperature of 1,350°C followed by cooling at 1°C/second to a test temperature between 1,300°C and 600°C with tests at every 50°C. Temperature was controlled using an S-type thermocouple welded to the midpoint of the sample. During the heating, homogenization and cooling, zero force on the sample was maintained through automatic control over the stroke position. At the test temperature, a constant stroke of 2.09 mm/minute was applied to give an approximate tensile strain rate of 1 x 10^{-3} second^{-1} until the specimen fractured. After fracture, the broken sample pieces were cooled by contact with the jaw grips. Specimens for metallography were obtained by quenching via jaw cooling at the end of the homogenization hold after cooling at 1°C/second to 750°C. Testing was performed under a high vacuum. Given limitation on total number of samples, three to five repeat tests were prioritized for the temperatures between 700°C and 1,000°C.

The percentage of reduced area (%RA) was determined by calculation using caliper measurements of the diameter of the original round bar and of the average of the minimum and maximum diameter of the broken specimen at the fracture surface. The distance from the thermocouple to the fracture surface was measured. Surface fractography was performed using optical macrographs as well as using a Zeiss EVO MA-10 scanning electron microscope (SEM) utilizing secondary electron mode. Subsurface fractography was carried out by sectioning parallel to the specimen axis, polishing, and etching with a 2% nital solution and viewed by optical microscopy (OM). The metallographic specimens were sectioned transverse to the sample axis at the thermocouple location (i.e., midpoint of specimen). These samples were polished and etched with 2% nital solution and observed with OM.

Figure 2

Hot ductility sampling schematic (a) and sample design (b).

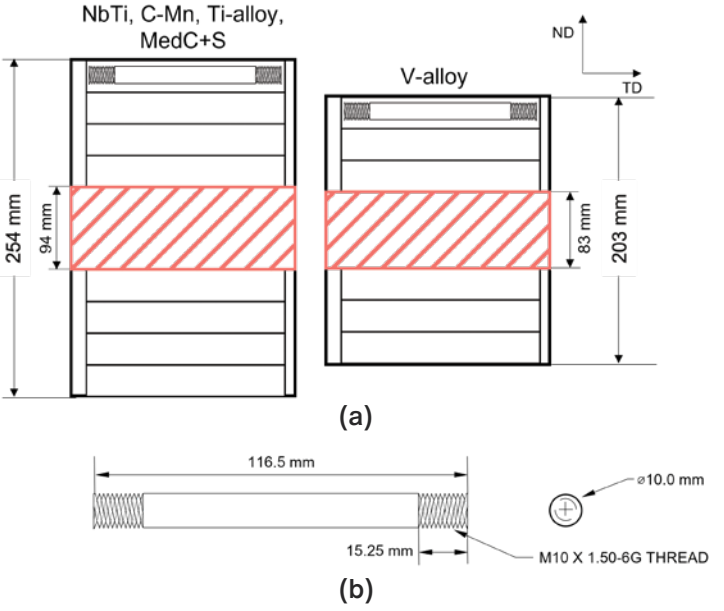

Also, metallography specimens were etched with saturated aqueous picric acid with a few drops of HCl and Agepon (wetting agent) added at room temperature then lightly back-polished with colloidal silica to reveal the prior austenite grain boundaries (PAGB) using OM. The prior austenite grain size (PAGS) was determined according to ASTM E112 using the comparison method as well as mean lineal intercept via Abrams Three-Circle Procedure.

The five steel grades in this study include: (1) a low-carbon microalloyed steel (NbTi), (2) a low-carbon steel (C-Mn), (3) a Ti-alloyed steel (Ti-alloy), (4) a V-alloyed steel (V-alloy), and (5) medium-carbon resulfurized

Figure 3

1,350°C homogenized hot ductility program.

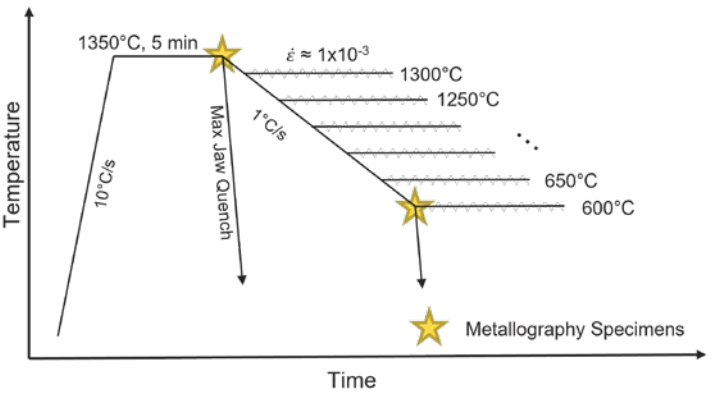

Table 1

Chemistries of Studied Steels

Steel	C wt.%	Mn wt.%	S ppm	Al wt.%	Ti wt.%	N ppm	Other elements	CE[13]
NbTi	0.058	1.42	Residual	0.043	0.022	<70	Nb	0.088
C-Mn	0.089	0.85	Residual	0.037	Residual	<100	—	0.111
Ti-alloy	0.177	0.38	Residual	0.038	0.02	<100	—	0.180
V-alloy	0.164	0.96	Residual	0.045	Residual	<100	V	0.202
MedC+S	0.407	0.83	0.0255	0.031	Residual	<100	V, Mo, Cr	0.432

low-alloy steel (MedC+S). These are listed in order of their carbon equivalence as determined by:[13]

$$\text{Ceq.} = \%C + 0.01\%Mn + 0.147\%S + 0.008\%P + 0.009\%Si + 0.007\%Cu + 0.02\%Ni + 0.003\%Cr + 0.009\%V + 0.04\%Nb + 0.007\%Mo + 0.05\%Al + 0.007\%Ti + 0.5\%Ni^{13}$$

where elemental weight percentages are used. The chemistries as determined by Leco analysis (C, S, N) and optical emission arc spectroscopy (other elements) and are presented with their carbon equivalency in Table 1. Thermo-Calc (TFCE 10 steel database[22]) was used to model the equilibrium phases and precipitates in each of the steels.

Results and Discussion

The Thermo-Calc equilibrium phases for the five steel grades are compared to a schematic Fe-CE (iron-carbon equivalent) phase diagram in Fig. 4. This figure provides context to the phase transitions expected in relation to one another. It is seen that steels C-Mn and Ti-alloy are expected to be close to and on either side of the peritectic reaction, though this study does not investigate the hot ductility issues that related to the peritectic reaction. Further details of the equilibrium phases as predicted by Thermo-Calc are given in Fig. 5. Here, the predicted differences in phase transformations and precipitates can be observed, which provides some expectation of where the ductility trough may form near Ae_3 for each steel.

The primary phase predictions reveal some differences are expected in the austenite to α-ferrite transition between the different grades. This is most notable in MedC+S with its significantly lower Ae_3 temperature. More on the austenite decomposition is discussed later in context of the hot ductility results. In terms of precipitates, NbTi and Ti-alloy steels show Ti(C,N-rich) precipitates that are stable at high temperatures. Steels C-Mn and V-alloy show significant amounts of the AlN phase are stable while steels Ti-alloy and MedC+S also shows a modest amount of AlN is predicted to be in equilibrium. Steel NbTi shows a significant amount of (Nb-rich,Ti)C are expected to form with increasing fraction as temperatures move lower. Substantial V(C,N) is predicted to be stable in MedC+S though V-alloy also shows their presence at the lower range of the austenite and α-ferrite transformation. The MedC+S also shows higher CaS with Ti-alloy having a modest amount as well.

The RA% results from the hot ductility tests are presented in Fig. 6 for each grade, including the individual

Figure 4

Schematic representation Fe-CE (iron-carbon equivalent[13]) phase diagram with the steel grades and the relative transition temperatures (liquidus, solidus, austenite start, α-ferrite start and austenite stop temperatures) calculated using Thermo-Calc (TCFE10 Steel database).

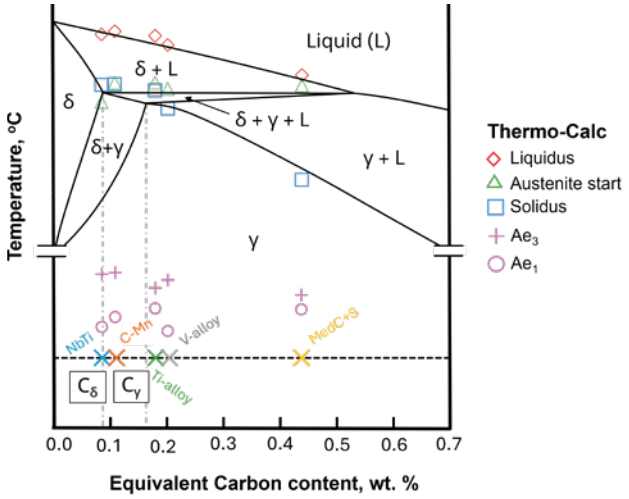

Figure 5

Equilibrium solidification phase predictions by Thermo-Calc[22] for all steel grades showing primary phases and precipitate phases of potential significance.

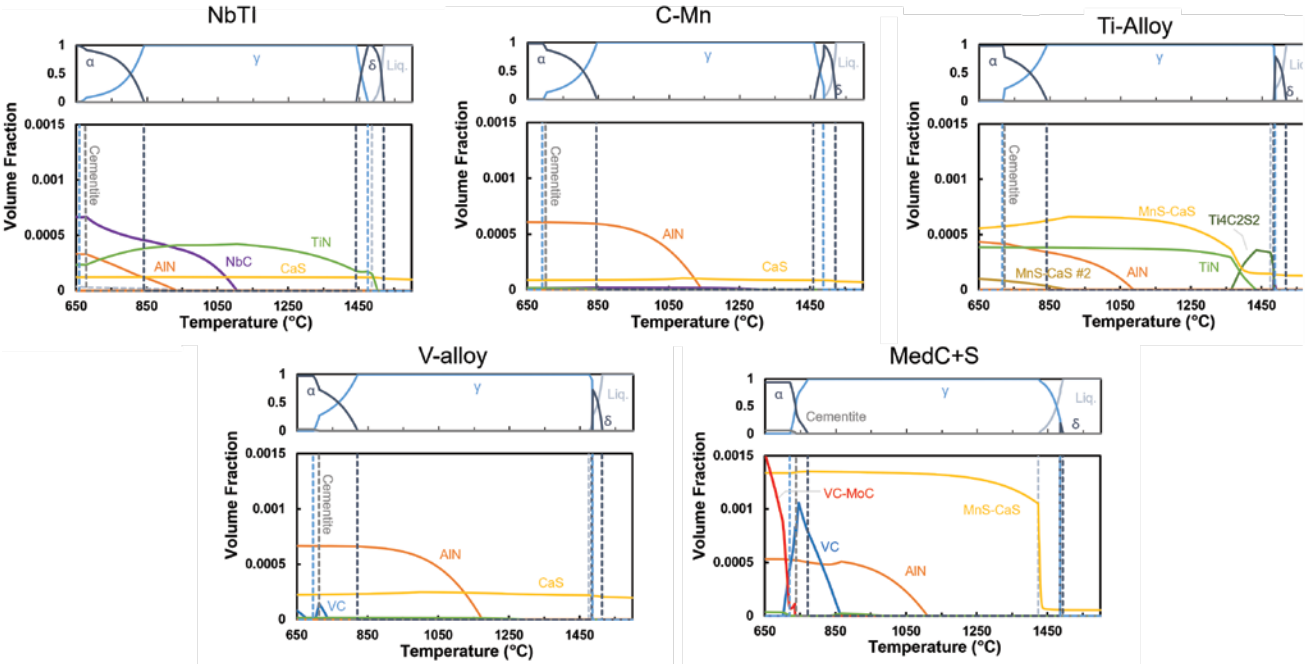

Figure 6

Hot ductility RA% results all steel grades.

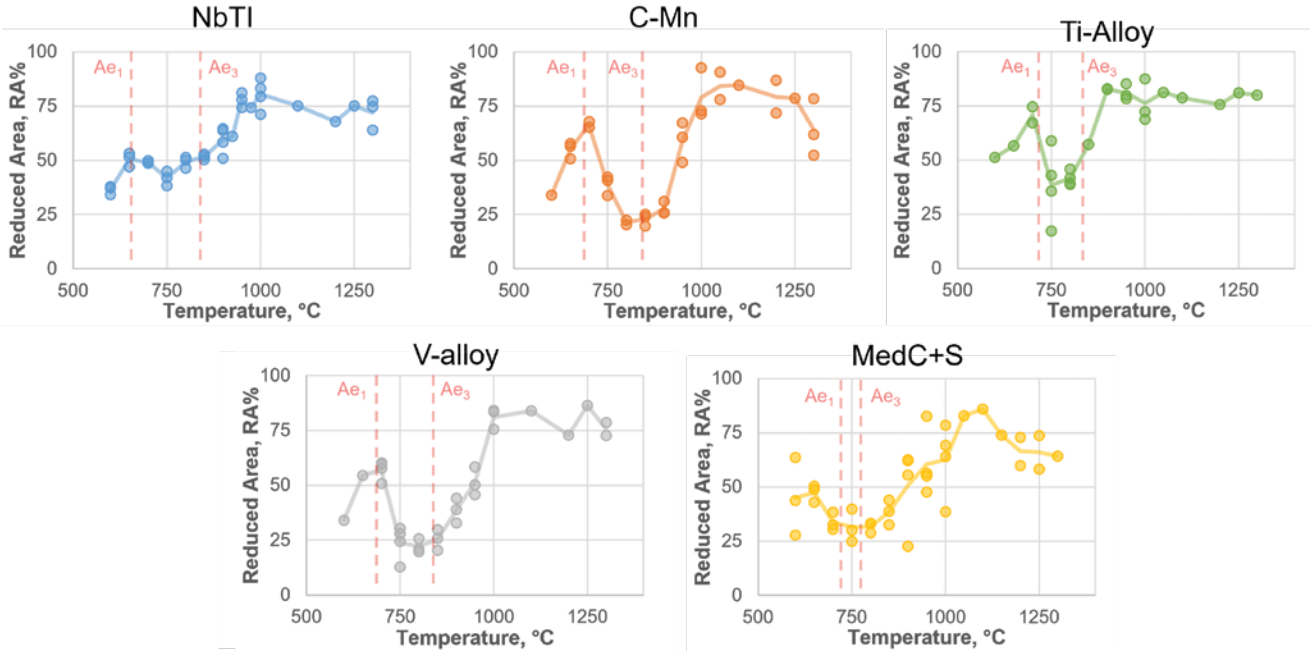

Figure 7

Fractography of steel NbTi at 950°C showing ductile fracture; surface images showing void coalescence (a–c), subsurface microscopy showing voids and damage close to fracture surface (right side) (d and e).

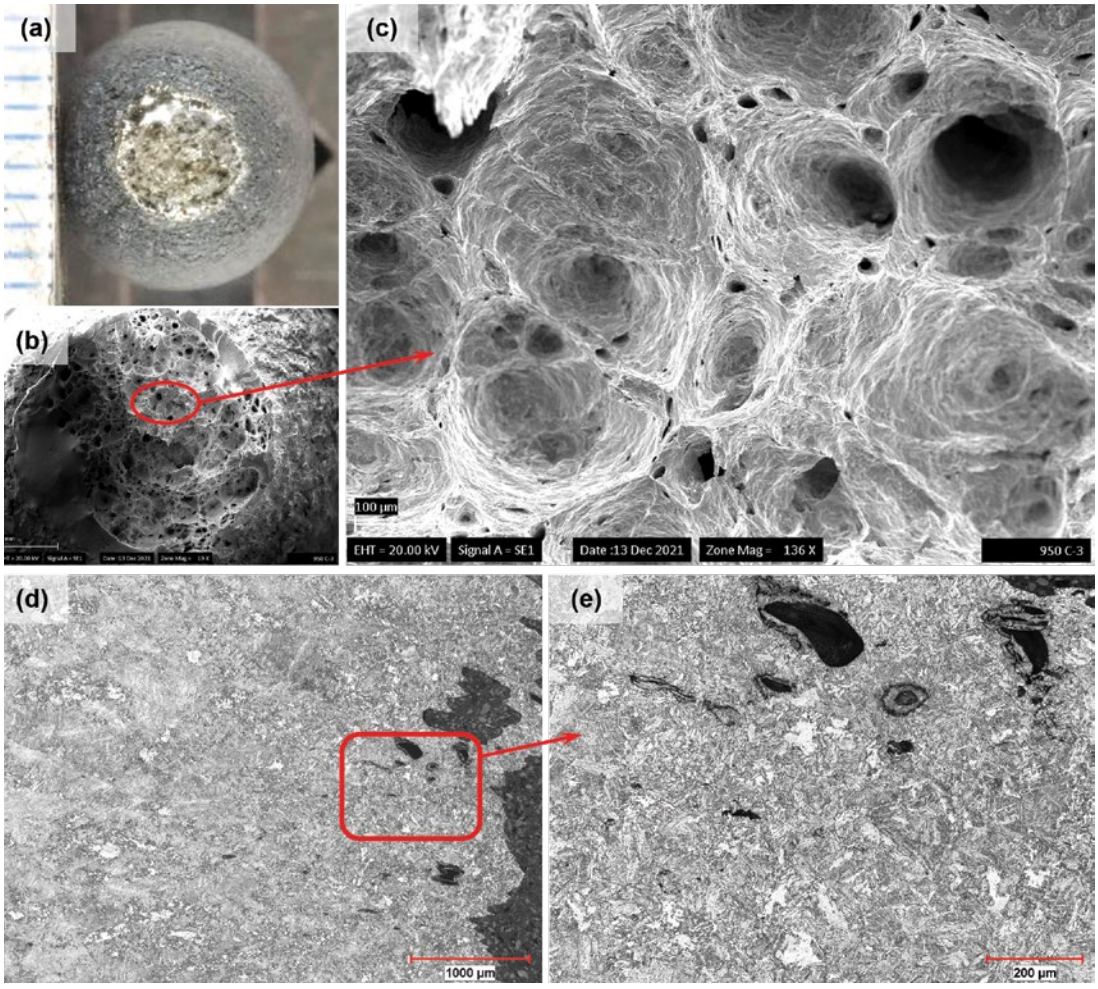

test points and a curve following the mean at each testing temperature. Steels NbTi and Ti-alloy show markedly better hot ductility performance compared to other steels with the average ductility trough minimum close to 40 RA%. Steels C-Mn and V-alloy show a significant ductility trough with the minimum average value in the range of 20–30 RA%. The MedC+S does show a ductility trough as well though its minimum average value is just above 30 RA%.

Fractographic investigations were carried out for numerous specimens of each grade at the surface and subsurface of broken specimens. Here, samples tested at 750°C, 850°C, 950°C and 1,000°C are reviewed. Ductile fracture behavior showing signs of growing microvoids is exemplified in Fig. 7 for NbTi tested at 950°C. Lower ductility failures were associated with intergranular fracture exhibiting subsurface cracking, as shown for example in Fig. 8 for V-alloy as tested at 750°C. In some cases, electrical arcing at the fracture surface occurred just after the specimen broke. While the surface was damaged in these situations, the subsurface still provided some insight. Results of the fractography investigations are presented in Table 2. The results suggest that for this test method and geometry, ductile failures are seen in tests with >50 RA% while intergranular failures are seen at ≤42 RA% with some amount of mixed fracture behavior likely overlapping at these bounds. All steels show ductile behavior at 1,000°C, while only NbTi and Ti-alloy show some amount of ductile fracture at 850°C. Steels NbTi (Ae_3 = 842°C and Ae_1 = 659°C) and C-Mn (Ae_3 = 846°C and Ae_1 = 693°C) show similar ferrite phase growth at PAGBs in the 750°C subsurface fractography images to what is shown in Fig. 8 for V-alloy (Ae_3 = 821°C and Ae_1 = 695°C) and may provide some insight to the intergranular fracture observed on these samples. For Ti-alloy (Ae_3 = 841°C and Ae_1 = 717°C), the extent of ferrite formation

Figure 8

Fractography of steel V-alloy at 750°C showing intergranular fracture; surface images showing jagged morphology (a–c), subsurface microscopy showing cracks at prior austenite grain boundaries (PAGBs) and associated ferrite films near fracture surface (right side) (d and e).

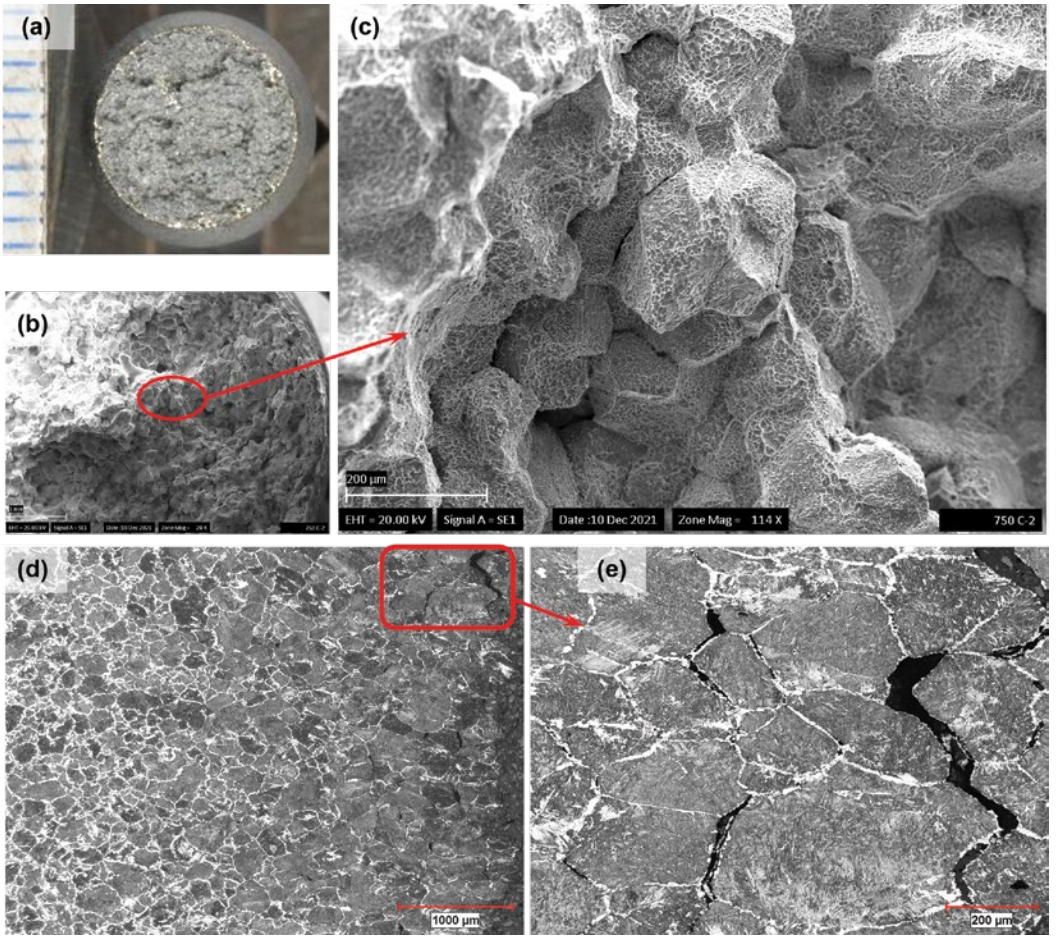

Table 2

Fractography Summary of Hot Ductility Tests. Surface fracture observations: IG = intergranular, MX = mixed, DC = ductile, NA = not available. Subsurface fracture morphologies: CR = cracks, MX = mixed, VD = voids

	750°C			850°C			950°C			1,000°C		
Steel	RA%	Surface	Sub-surface	RA%	Surface	Sub-surface	RA%	Surface	Sub-surface	RA%	Surface	Sub-surface
NbTi	42	IG	CR	50	MX	MX	74	DC	VD	79	NA	VD
C-Mn	34	IG	CR	20	IG	CR	61	DC	VD	71	DC	VD
Ti-alloy	36 59	IG DC	CR VD	57	DC	VD	85 55	NA NA	VD VD	73 88	NA NA	VD VD
V-alloy	28	IG	CR	20	IG	CR	50	DC	MX	84	DC	VD
MedC+S	40	MX	MX	39	IG	CR	23 63	NA DC	MX VD	79	DC	VD

Figure 9

Steel Ti-alloy showing different extent of transformation at 750°C; (a) 35.8 RA%, (b) 58.9 RA%.

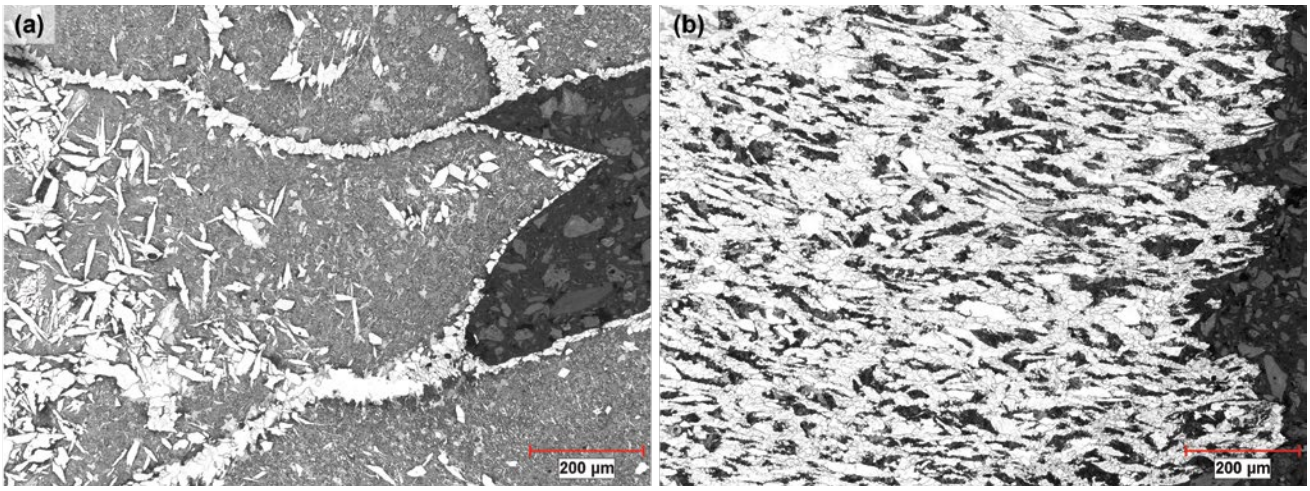

varied quite significantly between tests at 750°C as exemplified in Fig. 9. This variance also appears in Ti-alloy's scatter of RA% at this temperature, likely suggesting that the performance at these temperatures are sensitive to the extent of the austenite decomposition, possibly as a results of DIF as discussed in literature. Given that test temperatures were selected independent of material considerations, it is possible that this temperature happened to coincide strongly with this effect for Ti-alloy. If other steels were tested in a temperature close to the Ar_3 comparable to that observed for Ti-alloy, it is possible a similar sensitivity may be observed. The MedC+S (Ae_3 = 771°C and Ae_1 = 719°C) did not show ferrite growth at PAGBs for the 750°C likely due its lower austenite-ferrite equilibrium temperature.

Fitting its application, MedC+S intentionally had a significant amount of S. This S content did not appear to detract from overall hot ductility performance at least in comparison to steels C-Mn and V-alloy. However, it is seen that certain individual tests showed significantly worse results. Fractography on a sample showing particularly poor ductility is shown in Fig. 10. All samples of this grade showed some number of nonmetallic particles, however, Fig. 10b shows a large cluster of these particles at the surface. More generally, this specific sample showed more dispersed nonmetallic particles throughout the

Figure 10

Steel MedC+S at 750°C with poor hot ductility under scanning electron microscope (SEM) at low (a) and high (b) magnification.

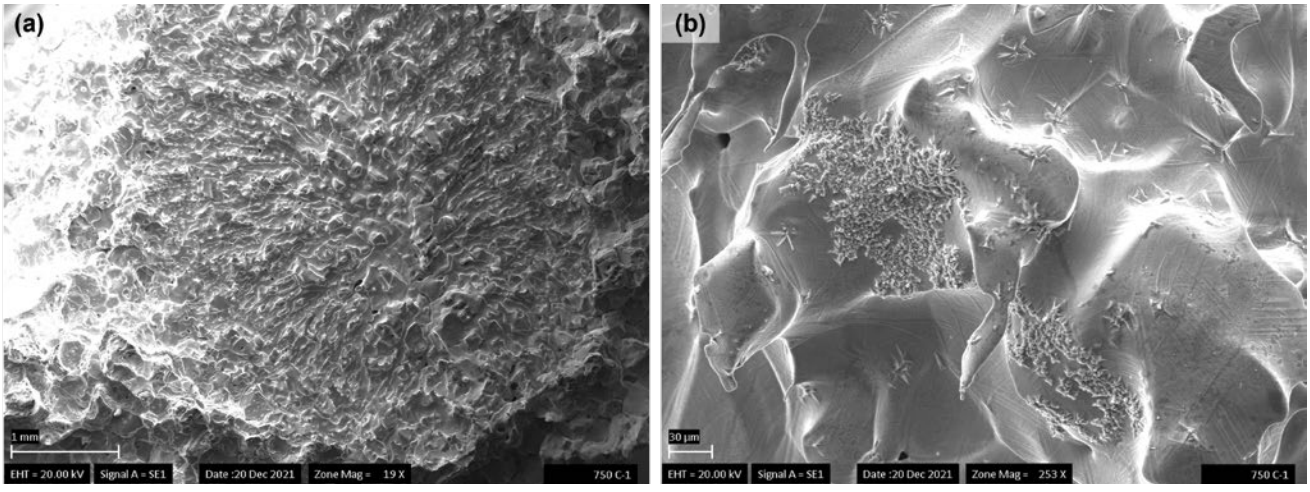

Figure 11

Prior austenite grain boundaries revealed in metallographic specimens of NbTi 750°C quench (a), C-Mn 750°C quench (b), Ti-alloy 1,350°C quench (c), V-alloy 750°C quench (d), and MedC+S 750°C quench (e).

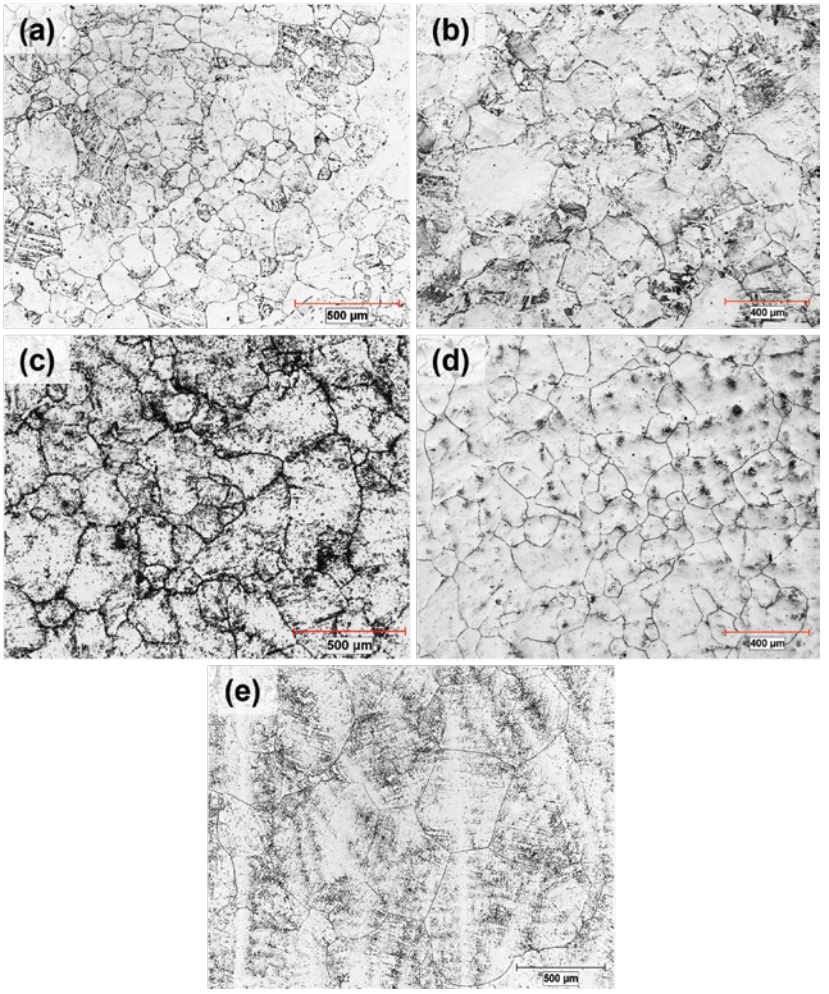

fracture surface. The better average ductility performance of this grade compared to C-Mn and V-alloy at low temperatures can be attributed to the formation of DIF triggered by MnS inclusions as indicated by Abushosha et al.[2] Thus, the overall hot ductility performance of MedC+S was good, but it should be expected to that local structures will arise at some frequency that increase crack susceptibility during casting.

To understand if the PAGS was a significant factor, the PAGBs were revealed as shown in Fig. 11. All steels but Ti-alloy had better quality etches in the 750°C samples compared to the 1,350°C samples, likely due to some amount of C segregation to PAGB. As confirmation that the 750°C PAGS can be used despite possible austenite decomposition, nital-etched microstructures at 750°C and 1,350°C were compared and showed all but Ti-alloy were reasonably comparable. The ASTM grain numbers and mean lineal intercept results for PAGS are given in Table 3. The PAGS results shows NbTi has a substantially finer grain size compared to the other grades. This is likely caused by the pinning behavior of stable TiN precipitates at the homogenization temperature (1,350°C) that are

Table 3

Prior Austenite Grain Size Measurements

	750°C quench		1,350°C quench	
Steel	ASTM grain size number	Mean lineal intercept (µm)	ASTM grain size number	Mean lineal intercept (µm)
NbTi	4.3	71.8	2.6	130
C-Mn	2.4	139	1.8	170
Ti-alloy	—	110	1.8	174
V-alloy	2.5	134	3.1	110
MedC+S	–0.5	378	-0.6	400

expected to have formed in this steel. The fine PAGS likely supported the good hot ductility behavior of NbTi. However, it is unclear how different the PAGS from this test is from the real scenario where the austenite forms at higher temperatures and so some caution is warranted with the results for this sample. Steel Ti-alloy also contains a similar level of Ti as the NbTi steel but shows a larger PAGS that is more comparable to C-Mn and V-alloy. In considering the Thermo-Calc predicted stability of the Ti-rich phase in Ti-alloy, it appears that this precipitate phase may be less stable at the homogenization temperature used and may have some coarsening or dissolution occurring that reduces the pinning of the austenite grain boundaries. Thus it appears that the good hot ductility results for Ti-alloy is not resultant from a fine PAGS when compared to the C-Mn and V-alloy steels. It is also apparent that MedC+S has a much larger PAGS than all other steels but has moderately better hot ductility results compared to C-Mn and V-alloy. This suggests that in all but NbTi, PAGS is not the dominant factor.

The influence of precipitate forming elements other than Ti such as Nb, V and Al is less clear. Only NbTi used a Nb addition but separating the influence of Nb from other factors such as the aforementioned fine PAGS for this steel is difficult. In any case, it appears that the Nb addition did not hinder hot ductility performance. Vanadium was used in both V-alloy and MedC+S, the latter of which used significantly more and showed a greater V(CN) content at low temperatures according to Thermo-Calc predictions. In the results, it does not appear that this was a singular dominating factor either as MedC+S had slightly better performance than V-alloy. The AlN equilibrium level predicted by Thermo-Calc does trend with results, but this study had no direct observation on the potential formation or effect of these precipitates making it difficult to conclude this the primary cause for the depth of the hot ductility trough.

As these steels were industrially produced using a scrap-based EAF process, residual elements were present. Of particular importance, the Cu level was noted to be higher NbTi, C-Mn, and V-alloy while all steels had a Ni to Cu ratio below 0.5. It is possible that the lower Cu values of Ti-alloy and MedC+S did assist hot ductility performance in comparison to C-Mn and V-alloy steel. In NbTi, the higher Cu content did not appear to be a determining factor perhaps due to other effects such as its finer PAGS or impact of Nb(CN) precipitation. Further investigation is needed to evaluate if the variation in Cu content of these grades was a factor in the hot ductility performance as these hot ductility tests conducted in a vacuum off a less severe oxidizing environment compared to actual casting conditions.[17]

Conclusions

Hot ductility testing on five steel grades was performed to provide a simple comparison of performance and crack susceptibility through secondary cooling and bending/straightening operations in a curved continuous caster. The results produced in this work matched operational experience well and are summarized as follows:

- The NbTi steel hot ductility performance was excellent, likely owing to a fine PAGS resulting from a TiN dispersion and the testing cycle applied.
- Good hot ductility was seen in the Ti-alloy steel despite having comparable PAGS to steels C-Mn and V-alloy, likely owing to a lesser amount of AlN formation. Variation in was seen in 750°C test where samples with more ferrite in the subsurface structure correlated with higher RA%.
- MedC+S had moderate hot ductility performance despite its medium C level, high S content and large PAGS. Test variation appeared to be related to the large number of nonmetallic particles (likely MnS).
- Steels C-Mn and V-alloy had relatively poorer hot ductility performance, possibly related to AlN formation.

Acknowledgments

The authors would like to thank the many contributors to this project at Interpro Pipe and Steel. In particular, Carl Dumonceaux, Colby Fafard, Kendal Dunnett, Maxim Fedin and Jing Su have been essential in acquiring material and data as well as central to discussions that guided this work.

References

1. M. Gontijo, C. Hoflehner, P. Estermann, S. Ilie, J. Six and C. Sommitsch, "Effect of Strain Rate on the Hot Ductility Behavior of a Continuously Cast Ti–Nb Microalloyed Steel," *Steel Research International,* Vol. 91, 2020, pp. 2000222–2000232.
2. R. Abushosha, S. Ayyad and B. Mintz, "Influence of Cooling Rate and MnS Inclusions on Hot Ductility of Steels," *Materials Science and Technology,* Vol. 14, No. 3, 1998, pp. 227–235.
3. M.H. Ghonchech, J. Sengupta, N. Wu, J. Gao and A.B. Phillion, "On the Hot Embrittlement of Continuously Cast and Transfer-Bar Structures in DP600 Advanced High-Strength Steel," *Journal of Materials Processing Tech.,* Vol. 189, 2021, pp. 116936–116945.
4. B. Mintz and A. Qaban, "The Influence of Precipitation, High Levels of Al, Si, P and a Small B Addition on the Hot Ductility of TWIP and TRIP Assisted Steels: A Critical Review," *Metals,* Vol. 12, 2022, pp. 502–531.

5. B. Mintz, R. Abushosha and J.J. Jonas, "Influence of Dynamic Recrystallization on the Tensile Ductility of Steels in the Temperature Range 700 to 1150°C," *ISIJ International,* Vol. 32, No. 2, 1992, pp. 241–249.
6. A. Rezian, "The Effect of Very High Temperature Deformation on the Hot Ductility of a V-Microalloyed Steel," 2008, McGill University.
7. B. Mintz, "Importance of Ar_3 Temperature in Controlling Ductility and Width of Hot Ductility Trough in Steels, and Its Relationship to Transverse Cracking," *Materials Science and Technology,* Vol. 12, No. 2, 1996, pp. 132–138.
8. A. Cowley, R. Abushosha and B. Mintz, "Influence of Ar_3 and Ae_3 Temperatures on Hot Ductility of Steels," *Materials Science Technology,* Vol. 14, No. 11, 1998, pp. 1145–1153.
9. J. Lewis, J.J. Jonas and B. Mintz, "The Formation of Deformation Induced Ferrite During Mechanical Testing," *ISIJ International,* Vol. 38, No. 3, 1998, pp. 300–309.
10. B. Mintz, R. Abushosha and M. Shaker, "Influence of Deformation Induced Ferrite, Grain Boundary Sliding, and Dynamic Recrystallization on Hot Ductility of 0.1-0.75%C Steels," *Materials Science and Technology.* Vol. 9, No. 10, 1993, pp. 907–914.
11. E. Essadiqi and J.J. Jonas, "Effect of Deformation on the Austenite-to-Ferrite Transformation in a Plain Carbon and Two Microalloyed Steels," *Metallurgical Transactions A,* Vol. 19A, No. 3, 1988, pp. 417–426.
12. K. Fudaba, et al. "Precipitation and Solution of Aluminum Nitride in Steel," *99th ISIJ Meeting,* 1980.
13. A. Normanton, "Improving Surface Quality of Continuously Cast Semis by an Understanding of Shell Development and Growth," *Technical Steel Research Series,* 1st ed., Luxembourg, 2005, p. 349.
14. G. Xia, H. Narzt, C. Fürst, K. Mörwald, J. Moertl, P. Reisinger and L. Lindenberger, "Investigation of Mould Thermal Behavior by Means of Mould Instrumentation," *Ironmaking and Steelmaking,* Vol. 31, 2004, pp. 364–370.
15. A. Howe, *Segregation and Phase Distribution During Solidification of Carbon, Alloy and Stainless Steels,* 1st ed., Commission of European Communities, Brussels, 1989, pp. 73–75.
16. Y. Maehara, K. Yasumoto, H. Tomono, T. Nagamichi, and Y. Ohmori, "Overview — Surface Cracking Mechanism of Continuously Cast Low Carbon Low Alloy Steel Slabs," *Material Science and Technology,* Vol. 6, 1990, pp. 793–806.
17. B. Mintz, "The Influence of Composition on the Hot Ductility of Steels and the Problem of Transverse Cracking," *ISIJ International,* Vol. 39, No. 9, 1999, pp. 833–855.
18. Z. Hongtao, L. Zhenand and W. Baorong, *Thermec-97, Int. Conf. on the Thermo-mechanical Processing of Steels and Other Materials,* eds. T. Chandra and T. Sakai, 1997, pp. 571–578.
19. Q. Yu, X. Yang, C. Lai and Z. Tang, "Study on MnS Inclusion Aggregation Along Continuous Casting Slab Thickness of Medium Carbon Structural Steel," *Metals,* Vol. 12, 2022, pp. 56–73.
20. H. Matsuoka, K. Osawa, M. Ono and M. Ohmura, "Influence of Cu and Sn on Hot Ductility of Steels With Various C Content," *ISIJ International,* Vol. 37, No. 3, 1998, pp. 255–262.
21. T. Kajitani, M. Wakoh, N. Tokumitsu, S. Ogibayashi and S. Mizoguchi, "Influence of Temperature and Strain on Surface Crack Due to Residual Copper in Carbon Steel," *15th PTD Conf. Proc.,* 1996, pp. 87–92.
22. Thermo-Calc Software TCFE Steels/Fe-alloys database version 10, accessed 6 June 2022.

AISTech This paper was presented at AISTech 2025 — The Iron & Steel Technology Conference and Exposition, Nashville, Tenn., USA, and published in the AISTech 2025 Conference Proceedings.

Did You Know?

Blastr Green Steel Receives Funding From Ecolab to Minimize Water Usage, Discharge

Water, hygiene and infection prevention solutions and services company Ecolab has invested in and will collaborate with Blastr Green Steel to develop water management systems at its steel plant in Inkoo, Finland.

The companies intend to work together to minimize seawater intake, seawater discharge and heat load to the sea. They estimate reductions of up to 85 to 90% and will explore further advances through stormwater integration and the use of municipal wastewater.

"Our collaboration has already created a path for Blastr to significantly reduce their water and energy use, limiting the project's environmental footprint and freeing up kilowatts for core process and production needs," said Thaís Gervasio, senior vice president and general manager of water solutions Europe at Ecolab.

The company said Ecolab has invested in the project and already begun to design the water management system. When the time comes, it will also build and operate it.

"Ecolab will work with us to design a water management system that advances Blastr's commitment to building a world-class steel mill with a significantly reduced environmental footprint," said Mark Bula, chief executive officer of Blastr Green Steel.